Effects of micropitted/nanotubular titania topographies on bone mesenchymal stem cell osteogenic differentiation

Lingzhou Zhao [a],[1], Li Liu [b],[1], Zhifen Wu [a], Yumei Zhang [c],**, Paul K. Chu [d],*

[a] Department of Periodontology and Oral Medicine, School of Stomatology, The Fourth Military Medical University, No. 145 West Changle Road, Xi'an 710032, China
[b] Department of Orthodontics, School of Stomatology, The Fourth Military Medical University, No. 145 West Changle Road, Xi'an 710032, China
[c] Department of Prosthetic Dentistry, School of Stomatology, The Fourth Military Medical University, No. 145 West Changle Road, Xi'an 710032, China
[d] Department of Physics and Materials Science, City University of Hong Kong, Tat Chee Avenue, Kowloon, Hong Kong, China

ARTICLE INFO

ABSTRACT

Micro/nanotopographical modification of biomaterials constitutes a promising approach to direct stem cell osteogenic differentiation to promote osseointegration. In this work, titania nanotubes (NTs) 25 and 80 nm in size with the acid-etched Ti topography (AcidTi) and hierarchical hybrid micropitted/nanotubular topographies (Micro/5VNT and Micro/20VNT) are produced to mimic the structure of the natural bone extracellular matrix (ECM). The effects on bone mesenchymal stem cell (MSC) osteogenic differentiation are studied systematically by various microscopic and biological characterization techniques. Cell adhesion is assayed by nucleus fluorescence staining and cell proliferation is studied by CCK-8 assay and flow cytometry. Osteogenic differentiation is assayed by alkaline phosphatase (ALP) expression, collagen secretion, matrix mineralization, and quantitative reverse transcription polymerase chain reaction (qRT-PCR) analysis on the osteogenesis related gene expression. All the topographies are observed to induce MSC osteogenic differentiation in the absence of osteogenic supplements. The nanotube surfaces significantly promote cell attachment and spread, collagen secretion and ECM mineralization, as well as osteogenesis-related gene expression. Among them, Micro/20VNT shows the best ability to simultaneously promote MSC proliferation and osteogenic differentiation. Our results unambiguously demonstrate their excellent ability to support MSC proliferation and induce MSC osteogenic differentiation, especially those with the micropitted topography.

© 2011 Elsevier Ltd. All rights reserved.

1. Introduction

Mesenchymal stem cells (MSCs) can give rise to a variety of adult cell types including osteoblasts [1,2]. They thus play important roles in many biological processes such as bone implant bio-integration [3,4] and constitute one of the most promising seed cells in bone tissue engineering [5]. Precise control of their differentiation to desired lineage is a key issue in stem cell research to promote implant bio-integration and regenerate tissues. It is recognized that the commitment of MSCs to specific lineage can be initiated by soluble chemical factors. For example, growth factors such as fibroblast growth factor (FGF)-2, bone morphogenetic proteins, and osteogenic supplements (OS) comprising dexamethasone, β-glycerophosphate,

and ascorbic acid can induce stem cell differentiation towards bone lineage [2,6]. However, it is difficult to deliver them in a reasonably controlled, combined, and spatiotemporal mode for a relatively long duration to attain satisfactory effects [7]. Furthermore, the growth factors used in most current research are usually at super-physiological doses in order to achieve obvious efficacy, but this inevitably raises safety concerns such as tumorigenicity. Though OS has shown stable and strong ability to induce stem cell osteogenic differentiation *in vitro*, the results cannot be extended to humans because they do not reflect the real situation *in vivo* and not much is known about the side effects of these chemicals [8,9]. Hence, it is important to identify safe and reliable alternative ways to manipulate stem cells.

Designing biomaterials surfaces possessing properties of natural extracellular matrix (ECM) to control the fate of stem cells has drawn enormous attention [10–13]. The physical properties of ECM such as micro/nanostructures play crucial roles in stem cell turn-over and commitment [14–16]. Therefore, biomaterials that can emulate the ECM structure are supposed to direct stem cell differentiation to a specific lineage similar to what natural ECM

does *in vivo* to yield good biological performance. In addition, the differentiation inducing ability originated from the topographical cues should be safer and more durable than the soluble factor delivery approach. Enlightened by the fact that the environment which cells encounter *in vivo* is a hierarchical structure comprising nano- to microscale constituents, biomaterials with micro- [13,17], nano- [8,12,18–23], or hybrid micro/nanoscale structures [24] have been fabricated to enhance stem cell functions. Among them, titania nanotubes (NTs) that can be fabricated with precisely controlled diameters and lengths have generated considerable interest [8,18–21,24–28]. They can be fabricated to mimic the dimensions of collagen fibril in bones [29] and elasticity of bones [30].In addition, other functional agents can be incorporated to further enhance the bioactivity [31,32] or confer other properties such as antibacterial ability [33]. By tuning the diameter of NTs, the available sites for cell integrin ligation can be changed and consequently, mechanotransduction and cell fate can be modulated [34–36]. Although the effects of NTs on stem cell behavior have been previously reported, there are conflicting results in the literature [8,19–21,37,38], and so before clinical application of NTs, their biological behavior must be better understood and an accurate understanding of their bioactivity is crucial. The hierarchical hybrid micro/nanoscale structures conjugating NTs with microtopography, which can better mimic the hierarchical structure of natural ECM, have been observed to promote more evenly multiple osteoblast functions [24], and so it is of special interest to observe whether they also exhibit beneficial effects on MSC functions.

In this work, the effects of NTs with two representative surface morphologies, namely the acid-etched microtopography and hierarchical hybrid micropitted/nanotubular topographies on MSC behavior are determined and their biological functions are evaluated. It should be mentioned that OS that is widely used in biomaterials/stem cell research to induce/accelerate osteogenic differentiation is not involved here because it may preclude or add uncertainty to accurate evaluation of materials bioactivity [8,9].

2. Materials and methods

2.1. Specimen preparation

Pure Ti foils ($10 \times 10 \times 1$ mm^3, Baoji Titanium Industry) were acid-etched and/or anodized according to previously described procedures [18,24]. In brief, the polished flat Ti samples (FlatTi) were anodized for 30 min in 0.5 wt% hydrofluoric acid (HF) at 5 and 20 V to form NTs of different tube sizes (denoted as 5VNT and 20VNT). Acid-etched Ti (AcidTi) was formed by acid-etching of FlatTi in 0.5 wt% HF for 30 min. AcidTi was further anodized at 5 and 20 V to form the hierarchical hybrid micropitted/nanotubular topographies (denoted as Micro/5VNT and Micro/20VNT). The micro- and nanoscale morphologies were examined by field-emission scanning electron microscopy (FE-SEM, HITACHI S-4800). All the Ti samples were sterilized by 30 min ultraviolet irradiation before use.

2.2. Cell cultures

The animal procedures were approved by the University Research Ethics Committee of The Fourth Military Medical University. The MSCs were obtained from the bone marrow of 2-week-old Sprague–Dawley rats. Briefly, after deep euthanasia and cervical dislocation, both femora and tibiae were dissected aseptically and soft tissues were detached.Then metaphysis from both ends were resected and the bone marrow contents were flushed out from the diaphysis with phosphate buffered saline (PBS, Gibco), collected by centrifuging, resuspended in a growth medium (GM) containing α-MEM (Gibco) and 10% fetal calf serum (FCS, Gibco), and cultured in a humidified atmosphere with 5% CO_2 at 37 °C. After 3 days, the medium was replaced with the non-adherent cells removed and thereafter the medium was changed every 3 days. When the culture grew to about 80% confluence, the MSCs were trypsinized using 0.25% trypsin (Sigma) and subcultured. The cells at passage 2–4 were used in the experiments.

2.3. Initial adherent cell number

The MSCs were seeded on the samples placed in 24 well plates at a density of 4×10^4 cells/well. After culturing for 0.5, 1 and 2 h, the adherent cells were fixed and stained with 4′,6′-diamidino-2-phenylindole (DAPI, Sigma) and then the cell numbers were counted in five random 5× fields on each sample under a fluorescence microscope (Leica).

2.4. Cell proliferation and cell cycle analysis

The MSCs were seeded on the samples placed in 24 well plates at a density of 2×10^4 cells/well, and after culturing for 1 and 4 d, cell proliferation was assessed using the CCK-8 assay. In brief, at the prescribed time points, the samples were rinsed with PBS and transferred to new 24 well plates. Then 300 ml of the α-MEM medium and 30 mL of the CCK-8 solution (Beyotime) were added to each sample and incubated at 37 °C for 2 h. The absorbance was measured at 450 nm.

The MSCs were inoculated on the samples at a density of 5×10^4 cells/cm^2 and after 24 h of culture, the cells on 8 samples of each group were trypsinized and pooled for cell cycle analysis. The cells were washed with PBS and resuspended in 1 mL of PBS by repeated vibration to get a suspension. Then the cells in the suspension were fixed with ice-cold dehydrated ethanol overnight at 4 °C. The fixed cells were washed twice with PBS and stained by 100 mg/mL propidium iodide (PI, Sigma) at 4 °C for 30 min. The PI-elicited fluorescence of individual cells was measured using Elite ESP flow cytometry (FCM, Becton Coulter). At least 40,000 cells were analyzed for each sample. The amounts of cells residing in the G0/G1 phase, S phase, and G2/M phase were determined.

2.5. Cell morphology

MSCs were seeded at a density of 2×10^4 cells/well. After 2 d of incubation, the samples with attached cells were washed with PBS, fixed in 3% glutaraldehyde, dehydrated in a graded ethanol series, freeze-dried, and sputter coated with gold prior to observation by FE-SEM. In order to display the effect of serum concentration on cell response to NTs, MSCs were cultured on FlatTi, 5VNT and 20VNT with 2%, 5% or 10% serum for 12 h and then the cell shape was examined by FE-SEM in the same way.

2.6. Alkaline phosphatase (ALP) staining, intracellular ALP activity and total protein synthesis

A cell suspension of 1 mL was seeded on each sample at a density of 2×10^4 cells/mL. After culturing for 3, 7, and 10 days, the cells were washed and fixed, and ALP staining was performed with the BCIP/NBT alkaline phosphatase color development kit (Beyotime) for 15 min. After culturing for 12 d, the cells were washed and lysed in 0.1 vol% Triton X-100. The alkaline phosphatase (ALP) activity in the lysis was determined through a colorimetric assay based on p-nitrophenyl phosphate (p-NPP). The intracellular total protein content was determined using a MicroBCA protein assay kit (Pierce) and the ALP activity was normalized to it.

2.7. Collagen secretion and ECM mineralization

Collagen secretion and ECM mineralization by the cells on the samples was assessed by the Sirius Red and Alizarin Red staining respectively [18,24]. 2×10^4 cells were added to each sample and cultured for 2 weeks. After washing with PBS and fixing, the constructs were stained using 0.1% Sirius Red (Sigma) to reveal the collagen or 40 mM Alizarin Red (pH 4.2, Solarbio) to show mineralization. The unbound stain was washed with 0.1 M acetic acid or distilled water before the images were taken. In the quantitative analysis, the Sirius Red or Alizarin Red stain on the specimen was dissolved in 0.2 M NaOH/methanol (1:1) or 10% cetylpyridinum chloride (Acros) to measure the optical density at 540 nm or 620 nm.

2.8. Gene expressions

The expression levels of osteogenesis related genes were measured using the quantitative reverse transcription polymerase chain reaction (qRT-PCR). The cells were seeded at a density of 2×10^4 cells/well, cultured for 2 weeks, and then harvested using TRIzol (Gibco) to extract RNA. An equivalent amount of RNA from each sample was reverse transcribed into complementary DNA (cDNA) using the Superscript II first-strand cDNA synthesis kit (Invitrogen). The qRT-PCR analysis of genes including ALP, osteocalcin (OCN), bone sialoprotein (BSP) and type 1 collagen (Col-1) was performed on the Applied Biosystems 7500 using the Quantitect Sybr Green Kit (Qiagen). The primers for the target genes were listed in Table 1. The expression levels of the target genes were normalized to that of the housekeeping gene GAPDH.

2.9. Statistical analysis

The one way ANOVA and Student-Newman-Keuls *post hoc* tests were used to determine the level of significance. $p < 0.05$ was set as significant and $p < 0.01$ was set as highly significant.

Table 1
Primers used for qRT-PCR.

Gene	Forward primer sequence (5′-3′)	Reverse primer sequence (5′-3′)
ALP	TTTGCTACCTGCCTCACTTCCG	GGCTGTGACTATGGGACCCAG
OCN	AGACTCCGGCGCTACCTCAACAAT	CAGCTGTGCCGTCCATACT
BSP	ACAGCTGACGCGGGAAAGTTG	ACCTGCTCATTTTCATCCACTTC
Col-1	CGTGACCAAAAACCAAAAGTGC	GGGGTGGAGAAAGGAACAGAAA
GAPDH	GGCACAGTCAAGGCTGAGAATG	ATGGTGGTGAAGACGCCAGTA

3. Results

3.1. SEM characterization

The morphologies of the fabricated samples were characterized by SEM (Fig. 1). At a lower magnification of 500×, FlatTi, 5VNT, and 20VNT appear relatively flat. Parallel grooves are present on FlatTi and sporadic small pits are observed from 5VNT and 20VNT. AcidTi, Micro/5VNT, and Micro/20VNT show a similar micropitted morphology, except that the sharp edges on AcidTi are smoothed slightly after anodization. Higher magnification pictures in the top right inset reveal the nanotopographies of the samples. FlatTi lacks obvious nanocues whereas the other samples have an evenly distributed nanotexture. 5VNT has an even distribution of tubes about 25 nm in diameter and one tube wall with a width of 5–10 nm is shared by two adjacent tubes. 20VNT has well separated tubes with a typical inner diameter of about 80 nm. The width of the tube wall is 10–20 nm and the gap between two adjacent tube walls is 20–50 nm. AcidTi shows an even distribution of nanodots about 20 nm in diameter and Micro/5VNT and Micro/20VNT exhibit a nanotubular texture similar to that of 5VNT and 20VNT.

3.2. Initial adherent cell number

The initial adherent cell number was measured by DAPI staining (Fig. 2). In general, no significant difference can be observed after culturing for 0.5, 1 and 2 h. Although the cell number on AcidTi appears to be larger than those on other samples at 0.5 h, there is no statistical significance.

3.3. Cell proliferation and cell cycle propagation

Cell proliferation was measured by the CCK-8 assay (Fig. 3a). At day 1, the MSC numbers on all the samples were slightly smaller
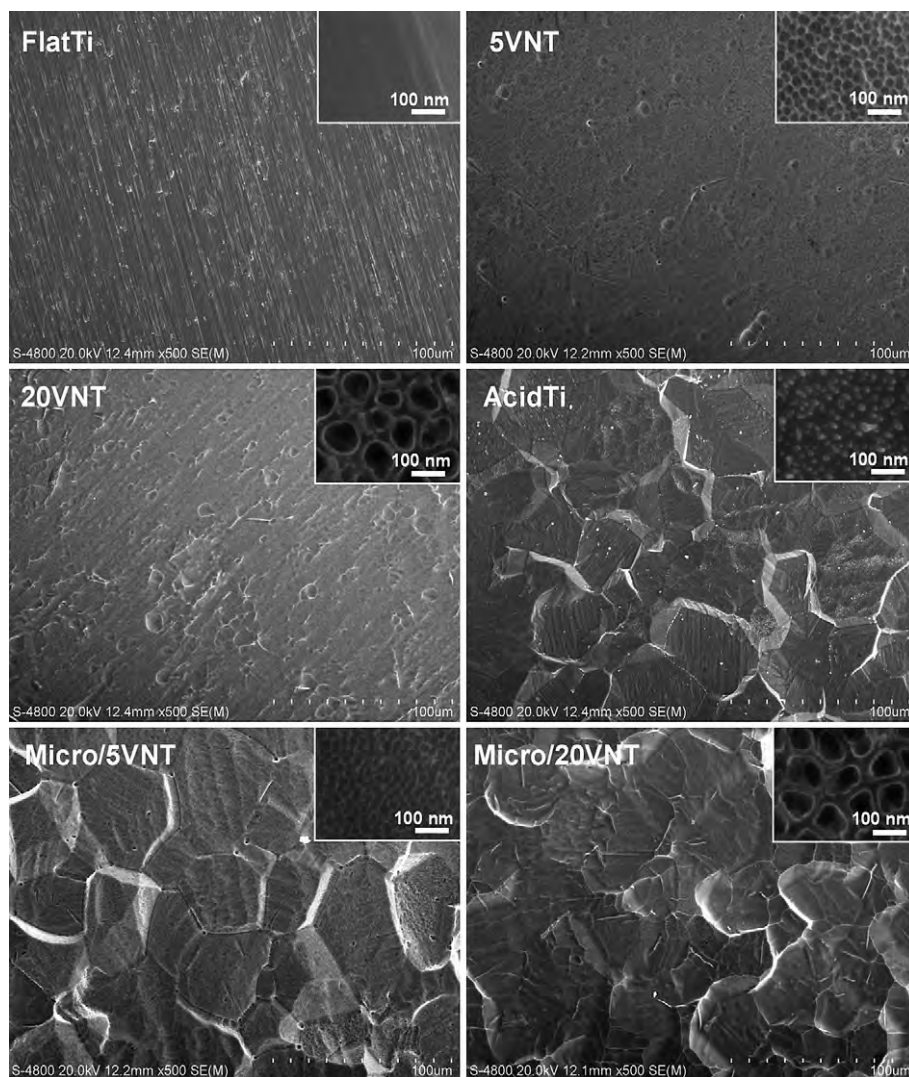

Fig. 1. SEM pictures of the fabricated Ti specimens. Pictures with a lower magnification of 500× display the overall microscale topography. The upper right insets of pictures show the images of a higher magnification of 100,000× to reveal the nanoscale texture.
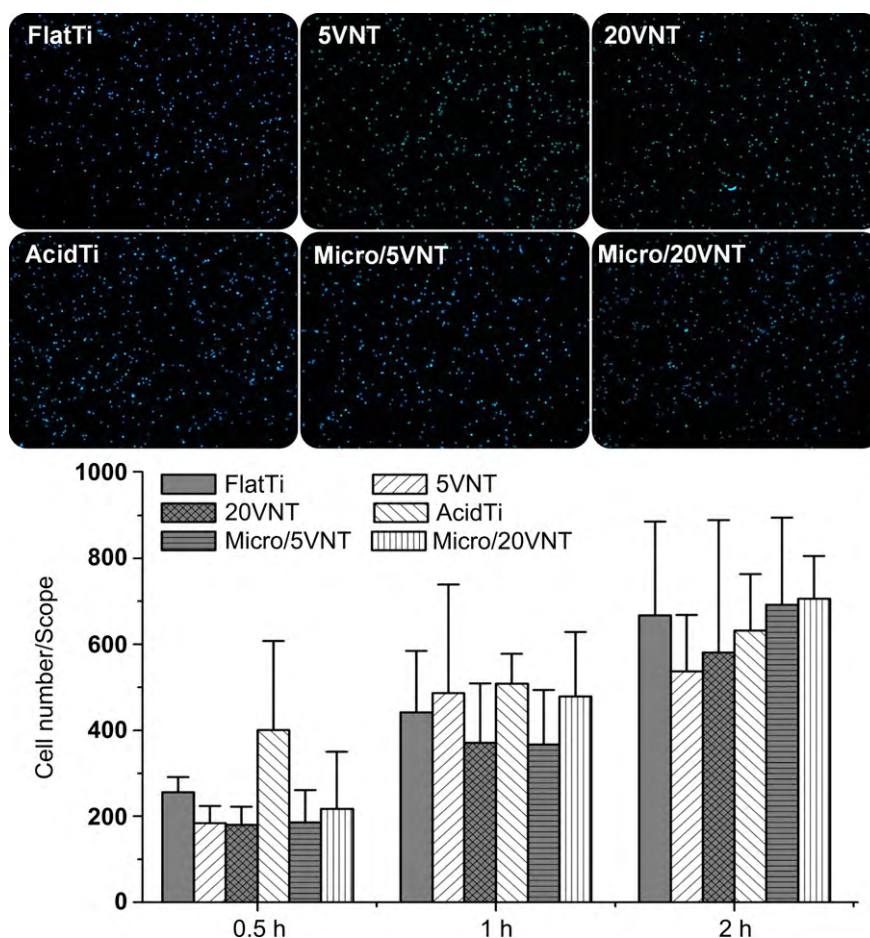
Fig. 2. Initial adherent MSC numbers measured by counting cells stained with DAPI under a fluorescence microscope after 0.5, 1 and 2 h of incubation. Upper panel shows the fluorescence images of cells attached after 1 h of incubation.

than that on FlatTi, while statistical significance was only observed from AcidTi and Micro/5VNT. The MSCs showed a time dependent growth pattern on all the samples. After culturing for 4 days, there was no obvious difference in the cell numbers among FlatTi, 5VNT, and 20VNT or among AcidTi, Micro/5VNT, and Micro/20VNT. However, the cell numbers on AcidTi, Micro/5VNT and Micro/20VNT were obviously larger than those on FlatTi, 5VNT and 20VNT.

The cell cycle propagation of MSCs was also monitored and the results are shown in Fig. 3b. AcidTi does not induce much difference in the percentage of S + G2M phases (40.9%) compared to FlatTi (41.76%). Addition of nanotubes slightly decreases the percentage of S + G2M phases irrespective of whether they are flat (38.29% for 5VNT and 34.04% for 20VNT) or rough (38.53% for Micro/5VNT and 34.52% for Micro/20VNT). There is no obvious difference between the flat and rough surfaces on the microscale for nanotubes of the same size. The bigger nanotubes show decreased percentage of S + G2M phases compared to the smaller nanotubes.

3.4. Cell morphology

The MSCs display dramatically different shapes related to the topography of the substrate, as shown in Fig. 4. Most of the MSCs on FlatTi have a small spindle fibroblast-like shape and spread poorly indicative of undifferentiated MSCs (Fig. 4a, b and c). The cells on AcidTi show similar spreading level to those on FlatTi but they have a polygonal geometry (Fig. 4m, n and o). In contrast, the cells on 5VNT, 20VNT, Micro/5VNT, and Micro/20VNT are more extended

with a polygonal osteoblast-like shape attached tightly to the substrate. The cell nuclei are clearly seen indicating good cell extension into the thin layer (Fig. 4f, j, r and v). Even on Micro/5VNT and Micro/20VNT where large microscale roughness exists, the cells still extend well and attach closely to the substrate along the micro/nanotexture (Fig. 4r, s, t, v, w and x). The higher magnification pictures disclose that the ECM deposited evenly following the nanotexture is mainly located at the top of tube walls and some of the tubes are covered by protein aggregates. The deposited proteins increase the widths of the top of the tube walls to 10–20 and 20–30 nm on 5VNT and 20VNT, respectively. The gaps between two neighboring tube walls on 20VNT are filled with the protein aggregates, resulting in intertubular areas 40–100 nm in width covered by proteins and available for cell focal adhesion formation. Accordingly, the holes shrink to be about 20 and 70 nm on 5VNT and 20VNT, respectively. We can see from the border of the cells that they preferably anchor to the intertubular area where proteins are available while avoiding the vacant holes (Fig. 4d and p).

3.5. ALP staining and intracellular ALP activity and total protein content

As shown in Fig. 5a, ALP production from the MSCs on all the substrates occurs as early as 3 days after incubation and increases with incubation time. There is no discernable difference in the ALP product among different samples at each time point. The assay results of intracellular ALP activity after 12 d of culture in Fig. 5b are
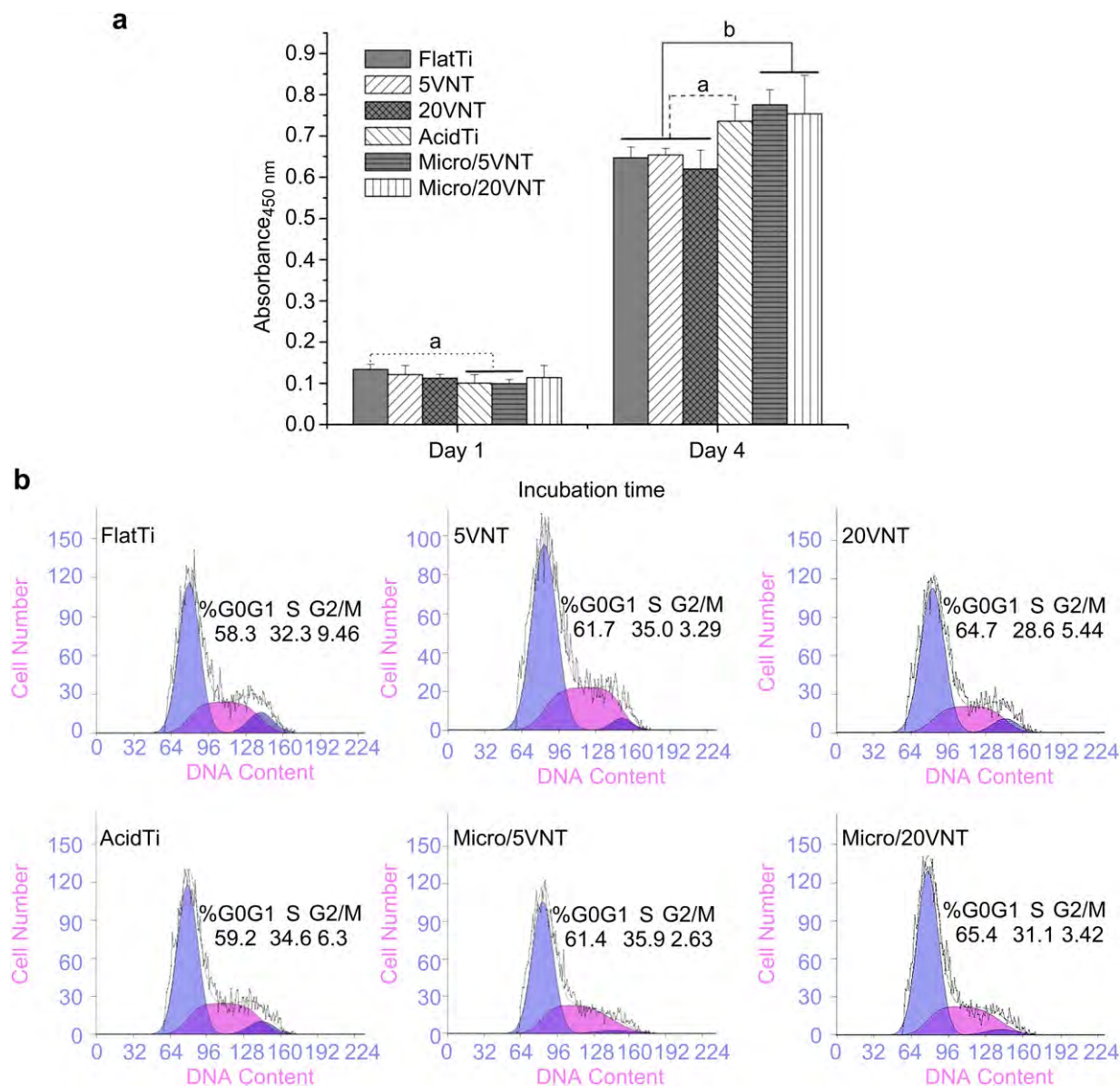
Fig. 3. (a) Cell proliferation measured by CCK-8 assay after culturing MSCs on different samples for 1 and 4 d with [a] $p < 0.05$ and [b] $p < 0.01$. (b) Representative cell cycle distribution graphs of MSCs cultured on different samples for 24 h, which were determined by FCM. The percentages of cells residing in the G0/G1 phase, S phase, and G2/M phase are shown in the graphs.

in accordance with the ALP staining results, showing no obvious difference in the ALP activity among different samples, except that the ALP activity on Micro/5VNT is lower than that on 5VNT. As shown in Fig. 5c, after culturing for 12 days, the intracellular total protein amounts on 20VNT, AcidTi, and Micro/20VNT are at the same level as that on FlatTi, whereas those on 5VNT and Micro/5VNT are slightly lower.

3.6. Collagen secretion

Collagen secretion was assessed by Sirius Red staining (Fig. 6). The optical images show that the MSCs secrete abundant collagen on all the samples after 2 weeks. The secreted collagen is denser on 5VNT, 20VNT, Micro/5VNT, and Micro/20VNT than on FlatTi and AcidTi. According to the quantitative results in Fig. 6, AcidTi induces slightly less collagen secretion than FlatTi but there is no statistical significance. Addition of nanotubes to

the Ti samples increases collagen secretion whether or not they are flat or rough on the microscale and the bigger nanotubes fare better than the smaller ones. Collagen secretion on Micro/5VNT and Micro/20VNT is obviously higher than that on 5VNT and 20VNT, respectively.

3.7. ECM mineralization

ECM mineralization was assessed by the Alizarin Red staining (Fig. 7). On FlatTi, there are small mineralization dots. However, 5VNT, 20VNT, AcidTi, Micro/5VNT, and Micro/20VNT induce abundant mineralization nodules that are much bigger than the mineralization dots on FlatTi. The quantitative results in the lower panel of Fig. 7 demonstrate that the ECM mineralization levels on 5VNT, 20VNT, MicroTi, Micro/5VNT, and Micro/20VNT are obviously higher than that on FlatTi, but no statistic difference is found among themselves.
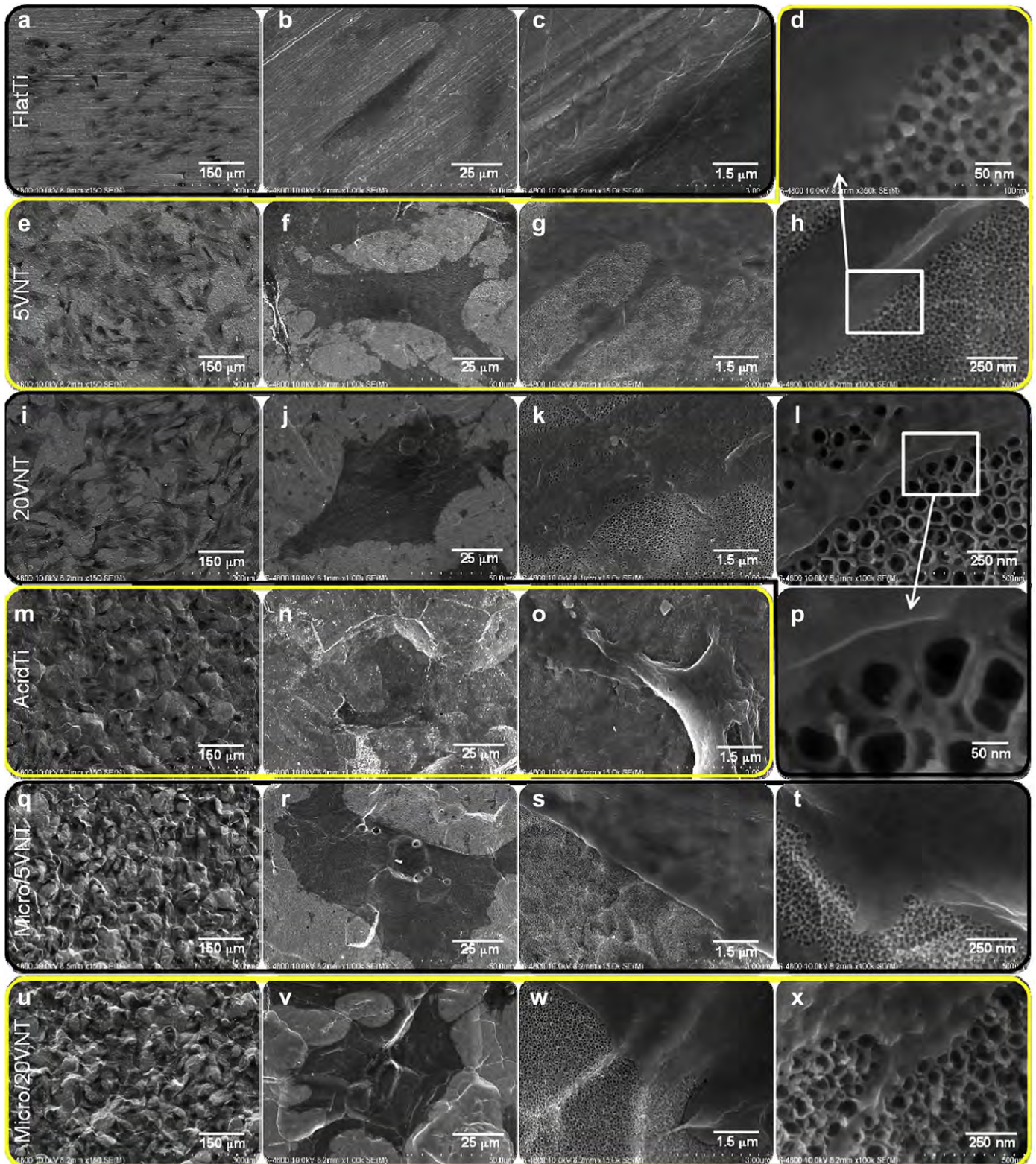
Fig. 4. SEM pictures showing the morphology of cells after 2 d of culture on samples. Pictures of with a low magnification of 150× (the first column) show the overall view. Pictures of 1000×(the second column) show the morphology of single cells and those of higher magnification (the two right columns) (15,000×, 100,000× except that d and p are 350,000× which are further magnification of h and l respectively) display the detail of cell interaction with the micro/nanotopographies.

3.8. Gene expressions

The expression levels of osteogenesis related genes including ALP, OCN, BSP, and Col-1 were assessed by the qRT-PCR with the results are shown in Fig. 8. The various topographies explored in this study induce different gene expression levels. Generally, 20VNT and Micro/20VNT induce the highest mRNA levels for all the osteogenesis related genes except Col-1.
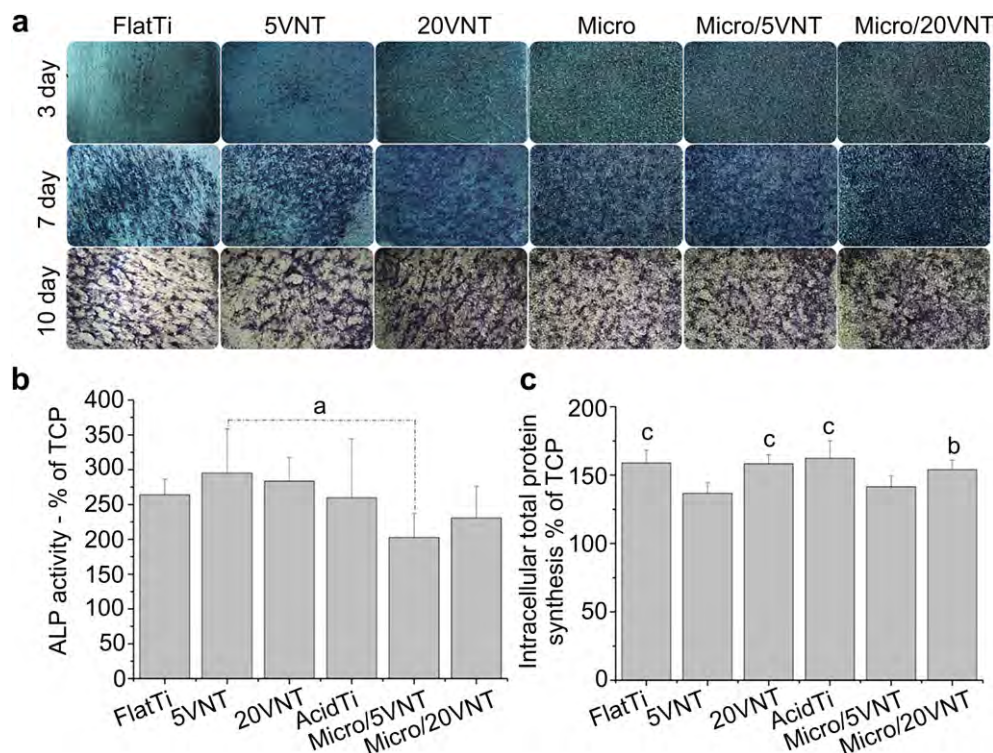
Fig. 5. (a) ALP staining of MSCs after 3, 7 and 10 d of culture. (b) ALP activity of MSCs on different samples cultured for 12 d, [a] $p < 0.05$. (c) Intracellular total protein synthesis of MSCs on different samples cultured for 12 d, [b] $p < 0.05$ and [c] $p < 0.01$ compared with 5VNT and Micro/5VNT.

4. Discussion

Biomimetic micro/nanotopographical modification is a promising approach to steer stem cell fate [8,12,13,17,19–23,39–42]. Nonetheless, although there have been reports concerning the effects of micro- and nanotopographies on stem cell differentiation, the overwhelming majority of them involve the exogenous stimuli such as OS [13,17,19–23,39–41] potentially confounding accurate assessment [8,9]. It has been suggested that more accurate evaluation may be accomplished by observing the sole role of topography without extra supplements [8,12,42]. NTs can give rise to better osseointegration especially after incorporation with the proper bioactive agents. However, the biological behavior of NTs is still not well understood [8,19–21] and the type of surface topography, that is, micro-, nano- or hierarchical hybrid micro/nanoscale, which can better induce stem cell osteogenic differentiation must still be clarified for optimization. Our results show that all the designed surface topographies, namely 5VNT, 20VNT, AcidTi, Micro/5VNT, and Micro/20VNT are capable of stimulating MSC osteogenic commitment in the absence of OS and among them, Micro/20VNT possesses the best ability. Our results provide more insights into the biological functions of micropitted/nanotubular topographies.

There is no obvious difference in the initial adherent cell numbers on different samples and it is consistent with our previous observation on osteoblasts [25]. The discordant results from Oh et al. that NTs induce larger initial cell numbers [8] may be attributed to autoclaving sterilization in their study compared to UV irradiation in our present work [18]. The cell cycle analysis results suggest that the nanotubes, especially those with a larger size, have a slight suppressive effect on early MSC proliferation. This proliferation suppressive effect is also mirrored by the cell proliferation assay results showing that at day 1, the cell numbers on all the topographies are slightly smaller than that on FlatTi. This slight proliferation suppressive effect is possibly related to the differentiation tendency

of MSCs because there is a reciprocal relationship between cell proliferation and differentiation [43]. In addition, the tight cell adhesion to the nanotube surfaces disclosed by the FE-SEM picture in Fig. 4 contributes partially to this effect, because cells need to detach slightly to undergo division and adhesion that is too strong will hinder this process. Nevertheless, the suppressive effect is neither serious nor long lasting on all the topographies. By day 4, the cell numbers on 5VNT and 20VNT are at the same level as that on FlatTi, and those on AcidTi, Micro/5VNT, and Micro/20VNT are obviously larger. The larger cell numbers on AcidTi, Micro/5VNT, and Micro/20VNT are possibly due to the larger surface area available for cell colonization. All in all, all the topographies can support stem cell growth and proliferation without showing any deleterious effect and among them, the surfaces with micropitted topography allow better cell proliferation.

All the surface morphologies in this study are capable of inducing MSC osteogenic differentiation in the absence of OS, as revealed by the increasing ALP product with incubation time and obvious ECM mineralized nodule formation. Though AcidTi gives rise to larger cell numbers and induces ECM mineralization nodule formation, it does not promote cell spread and slightly inhibits collagen secretion possibly giving rise to a smaller bone mass. In contrary, NTs strikingly promote cell spread, enhance collagen secretion, induce ECM mineralization, and up-regulate osteogenesis related gene expression. The larger 20VNT fares better here. NTs with the micropitted topography lead to even higher collagen secretion and simultaneously larger cell number. In general, Micro/20VNT shows the best ability. As aforementioned, the effects of NTs on the MSC fate are fiercely debated, as shown in Table 2 [8,19–21]. Park et al. demonstrated that small NTs of 15 nm enhanced cell activity while the larger ones of 50–100 nm impaired cell function and induced cell apoptosis [19,20]. However, Oh et al. observed that small NTs 30 nm in size promoted MSC adhesion without noticeable differentiation whereas larger ones 70–100 nm in size elicited
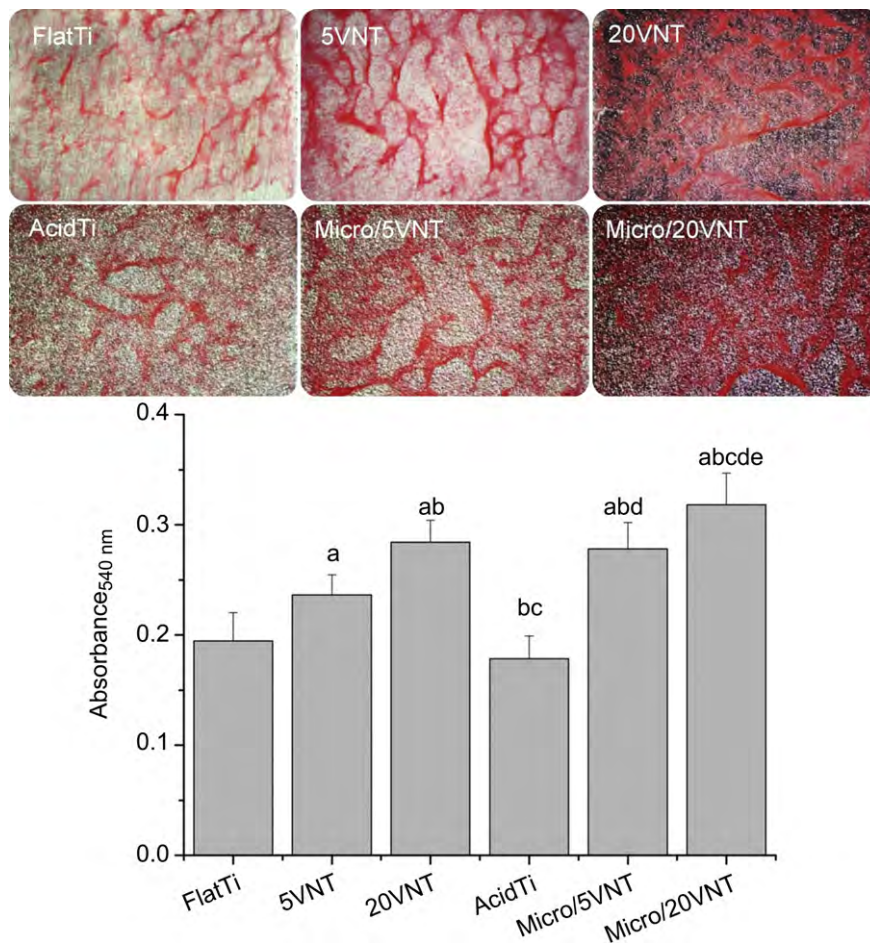
Fig. 6. Collagen secreted by MSCs on different samples after 2 weeks of incubation. The upper panel lists the optical images and the lower panel shows the quantitative colorimetric results. [a] $p < 0.01$ vs FlatTi; [b] $p < 0.01$ vs 5VNT; [c] $p < 0.01$ vs 20VNT; [d] $p < 0.01$ vs AcidTi; [e] $p < 0.01$ vs Micro/5VNT.

selective MSC differentiation to osteoblasts [8]. Popat et al. found that MSCs on the 80 nm NTs had higher adhesion, proliferation, and osteogenic differentiation [21]. Our results are in line with the latter two, corroborating that NTs are able to induce MSC osteogenic differentiation without the assistance of OS.The slightly disordered nanopits with a diameter of 120 nm on PMMA, a topography essentially similar to that of the NTs, were also observed to induce MSC osteogenic differentiation in the absence of OS by Dalby et al. [12]. Recently, Lavenus et al. also reported that titanium nanopores promoted osteogenic differentiation of MSCs in the absence of OS [44]. The two reports corroborate our results. Hence, most of the current evidence discloses that the NTs and similar structures are universal in inducing MSC osteogenic differentiation regardless of the substrate chemistry. The potential reasons for the conflicting results will be discussed later in this paper. Our observation that AcidTi also has the potential to induce MSC osteogenic differentiation is in line with a recent report by Olivares-Navarrete et al. [42]. The hierarchical hybrid micropitted/nanotubular structures Micro/5VNT and Micro/20VNT, showing a balanced promotion of multiple osteoblast functions [24], also simultaneously promote MSC proliferation and osteogenic differentiation. Our study provides a systematic comparison of the osteogenic inducing ability of NTs of different size, acid-etched topography, and hierarchical hybrid micropitted/nanotubular topographies. It is concluded that Micro/20VNT is most effective in inducing MSC osteogenic differentiation.

The micro/nanotopographies modulate cell shape [13] and focal adhesion [35,36,45], which alter the mechanotransduction including the indirect one, namely integrin dependent signal pathways and the direct one that is gene expressions, originate from cell nucleus distortion by force transferred *via* the cytoskeleton, thereby steering the cell fate [34,35,45,46]. The shape of stem cells on biomaterials is closely related to the high cytoskeletal tension, such as the well spread stem cell and that with the proper aspect ratio undergo osteogenesis, while the poorly spread stem cell becomes adipocytes [39,47,48]. Accordingly, the well spread polygonal shape of the MSCs on the nanotube surfaces predicts their fate concerning the osteogenic lineage, and the effect of nanotubes to promote MSC spread is an important mechanism in the osteogenesis inducing ability. As to the detailed mechanisms of the promoting effect of NTs on MSC attachment and spread on NTs, further studies are needed. The MSCs on AcidTi show a polygonal morphology attached to the curved microtopography, although they are not as well extended as those on the nanotube surfaces. This also results in increased cytoskeletal stress and the osteogenesis inducing ability of AcidTi, can be reasonably explained. The hierarchical hybrid micropitted/nanotubular structures give rise to better osteogenesis ability than the sole NTs. This is easy to understand because the close attachment of cells conforming to the microtopography leads to extra skeletal tension and mechanotransduction. The higher osteogenesis inducing ability of the 80 nm NTs than the 25 nm ones can be explained by the influence of the nanotopography on the cell focal adhesion size, distribution, and related mechanotransduction. The presentation of integrin ligation sites at a distance larger than a certain value (about 50−70 nm)
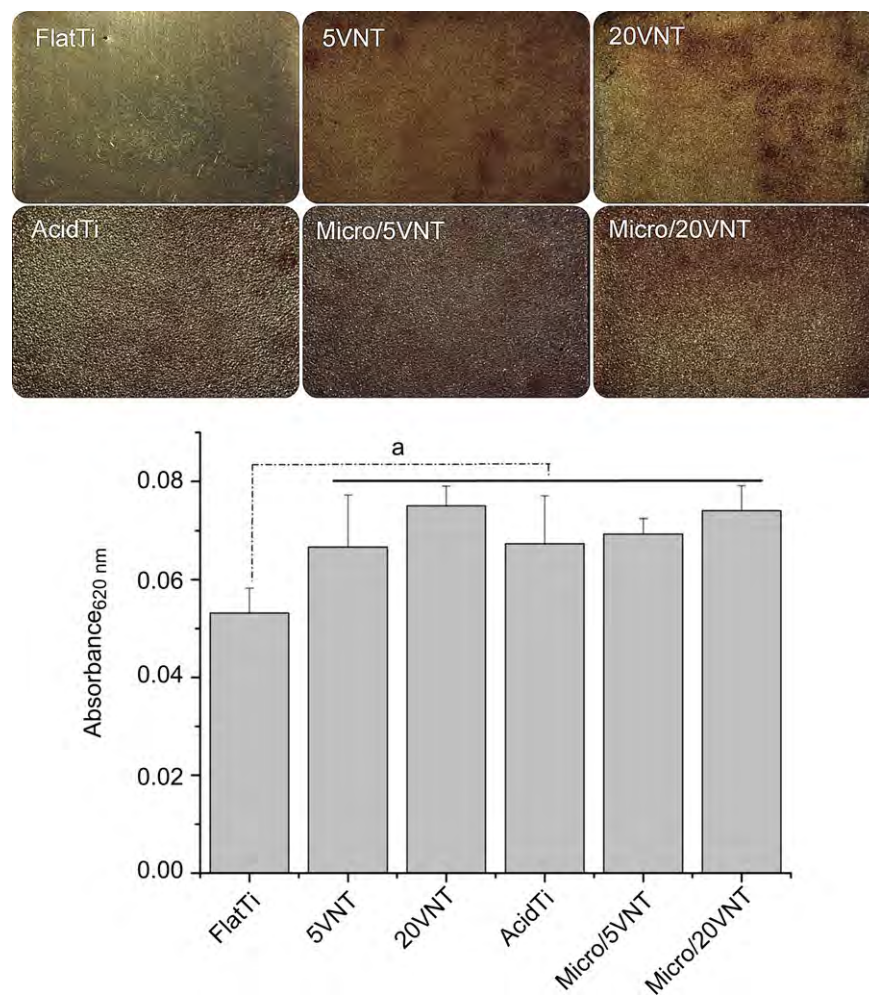
Fig. 7. ECM mineralization on different samples after 2 weeks culturing of MSCs. The upper panel shows the optical images and the lower panel displays the quantitative results with [a] $p < 0.01$.

perturbs integrin clustering, focal adhesion assembly, and organization of the actin stress fiber anchored to the focal adhesion [49,50]. Accordingly, the 25 nm NTs do not, or slightly, influence the integrin clustering and focal adhesion formation. Instead, the 80 nm NTs constrain the cell focal adhesion to the intertubular area. In this way, the 80 nm NTs modulate the size, shape, and distribution of focal adhesion to a nanoscale periodic occurrence. On the one hand, it triggers more integrin related signals, and on the other hand, it induces a nanoscale periodic distribution of cytoskeletal actin and stress leading to extensive nucleus distortion and related direct mechanotransduction signals [34]. To sum up, the micro/nanotopographies to a different extent regulate the cell shape as well as the size and distribution of focal adhesion to induce direct and indirect mechanotransduction thereby inducing MSC osteogenic differentiation.

The debate on whether NTs support MSC growth and induce osteogenic differentiation or lead to their apoptosis stems from the differences in the experimental conditions adopted by the different studies as shown in Table 2. Among these factors, the potential contribution of the annealing treatment to the conflict is ruled out by Park et al. [19]. Utilization of OS or not does not seem to account for the controversy either because it was adopted by Park et al. and Popat et al. but not by Oh et al. and ourselves.We have reported that the sterilization methods have significant influence on the bioactivity of NTs [18], but it does not appear to the main reason

(autoclaving used by Park et al. and Oh et al., ethanol immersion by Popat et al. and Park et al., and UV irradiation by us). We believe that the reason for the opposite result of Park et al. compared to others that small NTs 15 nm in size enhance cell activities while larger NTs with size of 50–100 nm induce cell apoptosis should be ascribed to the low serum concentration of 2% in the cell culture medium, and our observation in Fig. 9 verifies this conjecture. We have found that the different serum concentrations do not influence cell adhesion on FlatTi and 5VNT (Fig. 9a, b, e, f, i and j) but seriously affect that on 20VNT (Fig. 9c, g and k), suggesting that the serum concentration change alters the trend of the biological performance with NT size. The cells attach and spread well on 20VNT when cultured with 5% or 10% serum (Fig. 9g and k) while 2% serum leads to poor cell adhesion (Fig. 9c). This phenomenon can be explained by the cell adhesion mechanism. A requirement for normal cell functions on biomaterials is stable adhesion or else cell anoikis will occur [51], and thus the amount of adsorbed proteins is very important to the biological performance of biomaterials as they mediate cell adhesion. In our experiments, the amounts of proteins on the nanotopographies increase with serum concentrations from 2% to 10% (Fig. 9b, c, f, g, j and k). With regard to the flat surface and smaller NTs, because the focal adhesion assembly is not impaired and large microscale focal adhesion can form, the cells can attach and spread well in 10%, 5%, or 2% serum (Fig. 9a, b, e, f, i and j). As for the larger NTs with size of 50–100 nm,
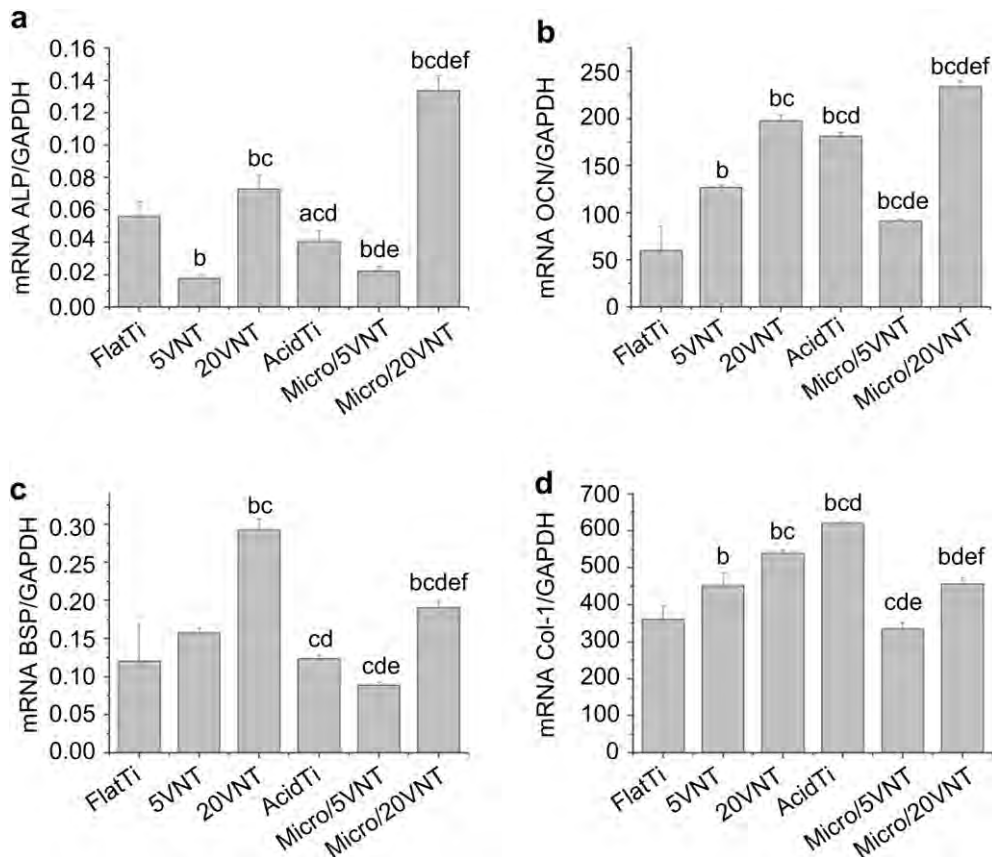
Fig. 8. Relative expressions of (a) ALP, (b) OCN, (c) BSP and (d) Col-1 by MSCs cultured on different substrates for 2 weeks, all values normalized to GAPDH. [a] $p < 0.05$ and [b] $p < 0.01$ vs FlatTi; [c] $p < 0.01$ vs 5VNT; [d] $p < 0.01$ vs 20VNT; [e] $p < 0.01$ vs AcidTi; [f] $p < 0.01$ vs Micro/5VNT.

as they constrain cell focal adhesion to the top of the tube walls, a high quality is needed for small focal adhesion to support stable cell adhesion. When cultured in 10% or 5% serum, the adsorbed proteins (Fig. 3 in Ref. [8], Fig. 4 in Ref. [21], Fig. 5 in Ref. [25], and Figs. 4 and 9f, g, j and k in present study) not only widen the intertubular areas, but also provide adequate integrin adhesion sites, giving rise to enough high-quality focal adhesion and good cell adhesion. In the 2% serum, the smaller amounts of adsorbed proteins (Fig. 3b in Ref. [20] and Fig. 9b and c in present study) result in narrow tube walls, a low density of integrin adhesion sites, low-quality small focal adhesion, and poor cell adhesion (Fig. 9c). Long and thin cell fillopodia are observed on 20VNT cultured in 2% serum indicating that cells cannot form stable adhesion (Fig. 9d), while strong and thick lamilipodia are observed from cells cultured in 5% or 10% serum demonstrating stable cell adhesion (Fig. 9h and l). We have also observed many cell fragments on 20VNT on the cell retraction path (inset in Fig. 9d), which may partly account for cell apoptosis. Therefore, the low medium serum concentration of 2% used in cell cultures should account for the unfavorable effect of larger NTs on MSC functions observed by Park et al. [19,20]. As there are abundant proteins *in vivo*, the results obtained from 10% serum should reflect the *in vivo* performance of NTs more accurately.

It should be pointed out that even among those reporting beneficial effects of NTs on MSC functions, the results of Oh et al. [8] are to a certain extent different from those of Popat et al. [21] and ours. Oh et al. demonstrated that the larger NTs elicited dramatic MSC elongation, while a well-spread polygonal shape was observed by Popat et al. and us. The reason for this discrepancy may be due to the different phenotypes of cells with a commercial cell strain used by Oh et al. while lab isolated cells were used by the others. There is

plenty of evidence from primary osteoblasts [25], osteoblast cell lines [26,27], endothelial cells [28], and vascular smooth muscle cells [28] that cells of different phenotypes respond differently to the same nanotopography. Our previous results concerning osteo-blasts [25] and the present study concerning MSCs jointly demonstrate the differential responses of the two types of cells to the NTs, and it is corroborated by a recent report from Brammer et al. [52]. It is thus highly possible that the commercial cell strain shows phenotypic differences from that of the lab isolated ones. More recent work done by the group of Oh et al. shows that the commercial osteoblast strain MC3T3-E1 has a similar morphology as the commercial MSC strain [26] and this supports our viewpoint. Hence, the cell phenotypic difference may be responsible for the different cell shapes on NTs in Oh et al.'s reports which are some-what different from those of Popat et al and ours.

Our present study sheds light on the debate concerning the biological behavior of NTs confirming their osteogenesis inducing ability and justifying their applications in clinical bone implants. Actually, there is more evidence about the beneficial effects of NTs on *in vivo* osseointegration [53–56], which can be better under-stood now with regard to their osteogenesis inducing property. Considering the bigger surface area provided by Micro/20VNT for cell colonization, the mechanical interlocking ability of the micro-pitted topography and balanced improvement of multiple cell functions for both osteoblasts and MSCs, Micro/20VNT should induce good *in vivo* osseointegration and our ongoing *in vivo* experiments in fact confirm this. Our results are also meaningful to bone tissue engineering. By adding the proper nanotubular cues, scaffolds with higher intrinsic osteoinductivity may be developed to accelerate tissue regeneration. The topographical cues have also

Table 2
Comparison of the main conclusion and main differences in the experimental conditions in the reports on MSC functions on NTs.

	Main conclusion	Main differences in the experimental conditions				
		NT annealing	Sterilization	MSC cell type	Culture serum concentration	OS application
Park et al. [19,20]	Small NTs (15 nm) enhance MSC activities while larger ones (50–100 nm) impair cell functions	Both annealing and not	70% ethanol or autoclaving	Rat MSCs isolated in lab	2% except osteogenic assay (10%)	Yes
Oh et al. [8]	Small NTs (30 nm) promote MSC adhesion without noticeable differentiation whereas larger ones (70–100 nm) dramatically elicit cell elongation and osteogenic differentiation	500 °C for 2 h	Autoclaving	Commercial human MSC strain	10%	No
Popat et al. [21]	MSCs on NTs (80 nm) show higher adhesion, proliferation, differentiation compared to control	500 °C	70% ethanol	Rat MSCs isolated in lab	10%	Yes
Our present study	NTs of both 25 and 80 nm dramatically promote MSC spread and induce osteogenic differentiation	No	UV irradiation	Rat MSCs isolated in lab	10%	No

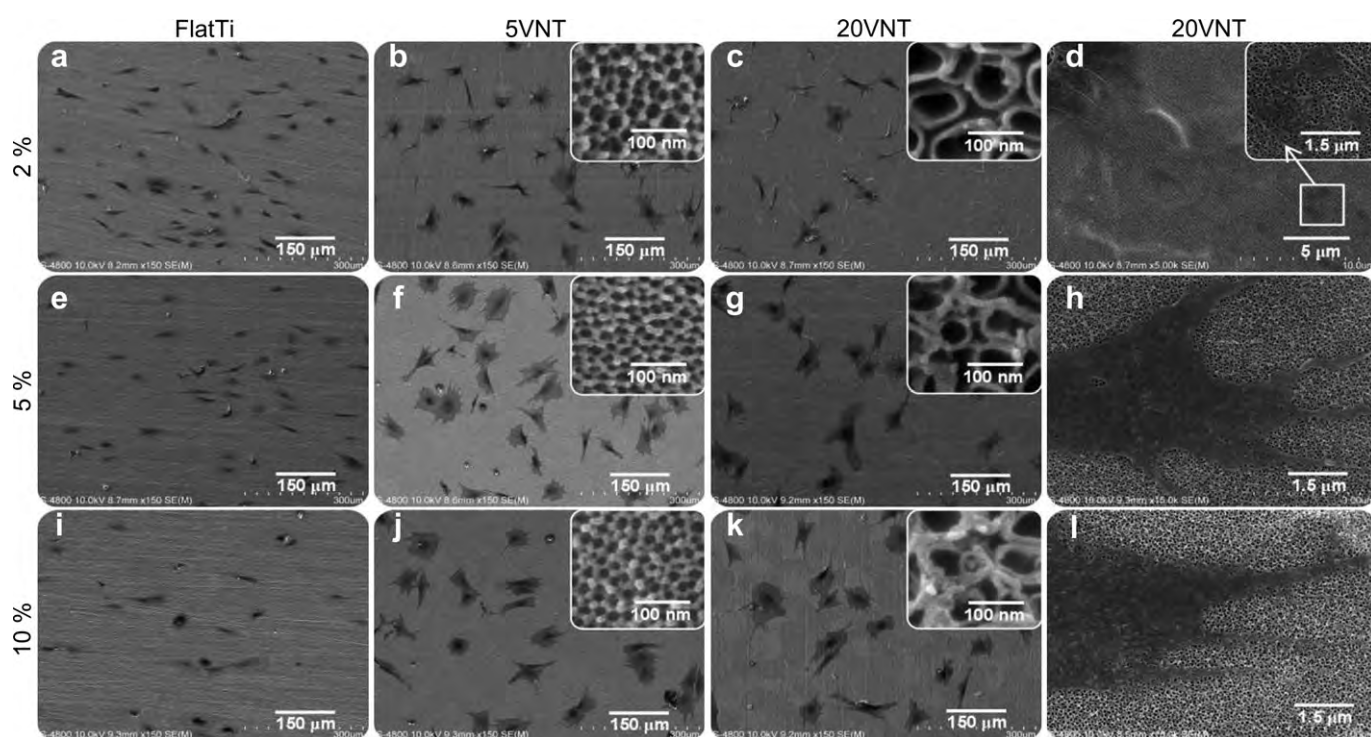**Fig. 9.** Cell shape on FlatTi, 5VNT and 20VNT cultured with 2%, 5% or 10% serum for 12 h displayed by FE-SEM. Figures are 150× except that Fig. d is 5000× and h and l are 15000×. The insets in b, c, f, g, j and k show the ECM deposition along the nanotopographies.

been reported to stimulate various soluble factors to secrete from attached cells [39,42] and it suggests the possibility of reconstructing bone cell niche comprising both topographical and soluble chemical cues merely through biomimetic topographical modification but obviating the complex exogenic growth factor administration. Such nanotubular cues containing scaffolds may induce better tissue regeneration either in the mode of scaffold/MSC co-cultures or more ideally *via* scaffolds alone through cell homing. This, especially the latter, facilitates clinical translation. Furthermore, it has been reported that porous calcium phosphate ceramics mimicking inorganic hydroxyapatites in bones [57] and biomimetic peptides mimicking organic proteins in bones [58] show good intrinsic osteoinductivity. Thus, bone implants and scaffolds with even better osteoinductivity can be prepared by combining the structure mimicking nanotubular cues and proper chemical simulation of the natural bone ECM.

5. Conclusion

Titania nanotubes (NTs) with sizes of 25 and 80 nm formed at 5 and 20 V (5VNT and 20VNT), acid-etched Ti topography (AcidTi), and hierarchical hybrid micropitted/nanotubular topographies (Micro/5VNT and Micro20VNT) mimicking the micro- and/or nanostructures of natural bone extracellular matrix (ECM) can induce MSC osteogenic differentiation in the absence of osteogenic supplements (OS). Among the samples, Micro/20VNT shows the best osteogenesis inducing ability which is related to the mechanotransduction alteration originated from cell extension and modulation of cell focal adhesion. Our results show that the different serum concentrations in the cell culture and cell phenotypic primarily account for the variations in the biological performance of NTs, demonstrating unambiguously that NTs can support MSC proliferation and induce MSC osteogenic differentiation. In

particular, results obtained from Micro/20VNT suggest immense potential in improving the clinical performance of bone implants.

Acknowledgements

References

[1] Pittenger MF, Mackay AM, Beck SC, Jaiswal RK, Douglas R, Mosca JD, et al. Multilineage potential of adult human mesenchymal stem cells. Science 1999; 284:143–7.

[2] Vater C, Kasten P, Stiehler M. Culture media for the differentiation of mesenchymal stromal cells. Acta Biomater 2011;7:463–77.

[3] Tasso R, Fais F, Reverberi D, Tortelli F, Cancedda R. The recruitment of two consecutive and different waves of host stem/progenitor cells during the development of tissue-engineered bone in a murine model. Biomaterials 2010;31:2121–9.

[4] Nair A, Shen J, Lotfi P, Ko CY, Zhang CC, Tang L. Biomaterial implants mediate autologous stem cell recruitment in mice. Acta Biomater 2011;7:3887–95.

[5] Caplan AI. Adult mesenchymal stem cells for tissue engineering versus regenerative medicine. J Cell Physiol 2007;213:341–7.

[6] Hwang NS, Varghese S, Elisseeff J. Controlled differentiation of stem cells. Adv Drug Deliv Rev 2008;60:199–214.

[7] Lee K, Silva EA, Mooney DJ. Growth factor delivery-based tissue engineering: general approaches and a review of recent developments. J R Soc Interface 2011;8:153–70.

[8] Oh S, Brammer KS, Li YS, Teng D, Engler AJ, Chien S, et al. Stem cell fate dictated solely by altered nanotube dimension. Proc Natl Acad Sci U S A 2009; 106:2130–5.

[9] Anderson JM, Vines JB, Patterson JL, Chen H, Javed A, Jun HW. Osteogenic differentiation of human mesenchymal stem cells synergistically enhanced by biomimetic peptide amphiphiles combined with conditioned medium. Acta Biomater 2011;7:675–82.

[10] Huebsch N, Arany PR, Mao AS, Shvartsman D, Ali OA, Bencherif SA, et al. Harnessing traction-mediated manipulation of the cell/matrix interface to control stem-cell fate. Nat Mater 2010;9:518–26.

[11] Engler AJ, Sen S, Sweeney HL, Discher DE. Matrix elasticity directs stem cell lineage specification. Cell 2006;126:677–89.

[12] Dalby MJ, Gadegaard N, Tare R, Andar A, Riehle MO, Herzyk P, et al. The control of human mesenchymal cell differentiation using nanoscale symmetry and disorder. Nat Mater 2007;6:997–1003.

[13] Guvendiren M, Burdick JA. The control of stem cell morphology and differentiation by hydrogel surface wrinkles. Biomaterials 2010;31:6511–8.

[14] Reilly GC, Engler AJ. Intrinsic extracellular matrix properties regulate stem cell differentiation. J Biomech 2010;43:55–62.

[15] Discher DE, Mooney DJ, Zandstra PW. Growth factors, matrices, and forces combine and control stem cells. Science 2009;324:1673–7.

[16] Guilak F, Cohen DM, Estes BT, Gimble JM, Liedtke W, Chen CS. Control of stem cell fate by physical interactions with the extracellular matrix. Cell Stem Cell 2009;5:17–26.

[17] Yang Y, Kusano K, Frei H, Rossi F, Brunette DM, Putnins EE. Microtopographical regulation of adult bone marrow progenitor cells chondrogenic and osteogenic gene and protein expressions. J Biomed Mater Res A 2010;95: 294–304.

[18] Zhao L, Mei S, Wang W, Chu PK, Wu Z, Zhang Y. The role of sterilization in the cytocompatibility of titania nanotubes. Biomaterials 2010;31:2055–63.

[19] Park J, Bauer S, Schmuki P, von der Mark K. Narrow window in nanoscale dependent activation of endothelial cell growth and differentiation on TiO$_2$ nanotube surfaces. Nano Lett 2009;9:3157–64.

[20] Park J, Bauer S, von der Mark K, Schmuki P. Nanosize and vitality: TiO$_2$ nanotube diameter directs cell fate. Nano Lett 2007;7:1686–91.

[21] Popat KC, Leoni L, Grimes CA, Desai TA. Influence of engineered titania nanotubular surfaces on bone cells. Biomaterials 2007;28:3188–97.

[22] Kaur G, Valarmathi MT, Potts JD, Jabbari E, Sabo-Attwood T, Wang Q. Regulation of osteogenic differentiation of rat bone marrow stromal cells on 2D nanorod substrates. Biomaterials 2010;31:1732–41.

[23] You MH, Kwak MK, Kim DH, Kim K, Levchenko A, Kim DY, et al. Synergistically enhanced osteogenic differentiation of human mesenchymal stem cells by culture on nanostructured surfaces with induction media. Biomacromolecules 2010;11:1856–62.

[24] Zhao L, Mei S, Chu PK, Zhang Y, Wu Z. The influence of hierarchical hybrid micro/nano-textured titanium surface with titania nanotubes on osteoblast functions. Biomaterials 2010;31:5072–82.

[25] Zhao L, Mei S, Wang W, Chu PK, Zhang Y, Wu Z. Suppressed primary osteoblast functions on nanoporous titania surface. J Biomed Mater Res A 2011;96: 100–7.

[26] Brammer KS, Oh S, Cobb CJ, Bjursten LM, van der Heyde H, Jin S. Improved bone-forming functionality on diameter-controlled TiO$_2$ nanotube surface. Acta Biomater 2009;5:3215–23.

[27] Popat KC, Eltgroth M, Latempa TJ, Grimes CA, Desai TA. Decreased Staphylococcus epidermis adhesion and increased osteoblast functionality on antibiotic-loaded titania nanotubes. Biomaterials 2007;28:4880–8.

[28] Peng L, Eltgroth ML, LaTempa TJ, Grimes CA, Desai TA. The effect of TiO$_2$ nanotubes on endothelial function and smooth muscle proliferation. Biomaterials 2009;30:1268–72.

[29] Tzaphlidou M. The role of collagen in bone structure: an image processing approach. Micron 2005;36:593–601.

[30] Crawford GA, Chawla N, Das K, Bose S, Bandyopadhyay A. Microstructure and deformation behavior of biocompatible TiO$_2$ nanotubes on titanium substrate. Acta Biomater 2007;3:359–67.

[31] Balasundaram G, Yao C, Webster TJ. TiO$_2$ nanotubes functionalized with regions of bone morphogenetic protein-2 increases osteoblast adhesion. J Biomed Mater Res A 2008;84:447–53.

[32] Xin Y, Jiang J, Huo K, Hu T, Chu PK. Bioactive SrTiO$_3$ nanotube arrays: strontium delivery platform on Ti-based osteoporotic bone implants. ACS Nano 2009;3:3228–34.

[33] Zhao L, Wang H, Huo K, Cui L, Zhang W, Ni H, et al. Antibacterial nanostructured titania coating incorporated with silver nanoparticles. Biomaterials 2011;32:5706–16.

[34] Curtis AS, Dalby M, Gadegaard N. Cell signaling arising from nanotopography: implications for nanomedical devices. Nanomedicine 2006;1:67–72.

[35] McNamara LE, McMurray RJ, Biggs MJ, Kantawong F, Oreffo RO, Dalby MJ. Nanotopographical control of stem cell differentiation. J Tissue Eng 2010; 2010:120623.

[36] Biggs MJ, Richards RG, Dalby MJ. Nanotopographical modification: a regulator of cellular function through focal adhesions. Nanomedicine 2010;6: 619–33.

[37] von der Mark K, Bauer S, Park J, Schmuki P. Another look at "Stem cell fate dictated solely by altered nanotube dimension. Proc Natl Acad Sci U S A 2009; 106. E60.

[38] Oh S, Brammer KS, Li YSJ, Teng D, Engler AJ, Chien S, et al. Reply to von der Mark, et al.: Looking further into the effects of nanotube dimension on stem cell fate. Proc Natl Acad Sci U S A 2009;106. E61.

[39] Kilian KA, Bugarija B, Lahn BT, Mrksich M. Geometric cues for directing the differentiation of mesenchymal stem cells. Proc Natl Acad Sci U S A 2010;107: 4872–7.

[40] Mendonca G, Mendonca DB, Simoes LG, Araujo AL, Leite ER, Duarte WR, et al. The effects of implant surface nanoscale features on osteoblast-specific gene expression. Biomaterials 2009;30:4053–62.

[41] Kim EJ, Boehm CA, Mata A, Fleischman AJ, Muschler GF, Roy S. Post microtextures accelerate cell proliferation and osteogenesis. Acta Biomater 2010;6: 160–9.

[42] Olivares-Navarrete R, Hyzy SL, Hutton DL, Erdman CP, Wieland M, Boyan BD, et al. Direct and indirect effects of microstructured titanium substrates on the induction of mesenchymal stem cell differentiation towards the osteoblast lineage. Biomaterials 2010;31:2728–35.

[43] Stein GS, Lian JB, Owen TA. Relationship of cell growth to the regulation of tissue-specific gene expression during osteoblast differentiation. FASEB J 1990;4:3111–23.

[44] Lavenus S, Berreur M, Trichet V, Louarn G, Layrolle P. Adhesion and osteogenic differentiation of human mesenchymal stem cells on titanium nanopores. Eur Cell Mater 2011;22:84–96.

[45] Biggs MJ, Richards RG, Gadegaard N, Wilkinson CD, Oreffo RO, Dalby MJ. The use of nanoscale topography to modulate the dynamics of adhesion formation in primary osteoblasts and ERK/MAPK signalling in STRO-1+ enriched skeletal stem cells. Biomaterials 2009;30:5094–103.

[46] Rape AD, Guo WH, Wang YL. The regulation of traction force in relation to cell shape and focal adhesions. Biomaterials 2011;32:2043–51.

[47] McBeath R, Pirone DM, Nelson CM, Bhadriraju K, Chen CS. Cell shape, cytoskeletal tension, and RhoA regulate stem cell lineage commitment. Dev Cell 2004;6:483–95.

[48] Peng R, Yao X, Ding J. Effect of cell anisotropy on differentiation of stem cells on micropatterned surfaces through the controlled single cell adhesion. Biomaterials 2011;32:8048–57.

[49] Cavalcanti-Adam EA, Volberg T, Micoulet A, Kessler H, Geiger B, Spatz JP. Cell spreading and focal adhesion dynamics are regulated by spacing of integrin ligands. Biophys J 2007;92:2964–74.

[50] Arnold M, Cavalcanti-Adam EA, Glass R, Blummel J, Eck W, Kantlehner M, et al. Activation of integrin function by nanopatterned adhesive interfaces. Chemphyschem 2004;5:383–8.

[51] Zhao L, Hu L, Huo K, Zhang Y, Wu Z, Chu PK. Mechanism of cell repellence on quasi-aligned nanowire arrays on Ti alloy. Biomaterials 2010;31:8341–9.

[52] Brammer KS, Choi C, Frandsen CJ, Oh S, Johnston G, Jin S. Comparative cell behavior on carbon-coated TiO$_2$ nanotube surfaces for osteoblasts vs. osteoprogenitor cells. Acta Biomater 2011;7:2697–703.

[53] von Wilmowsky C, Bauer S, Lutz R, Meisel M, Neukam FW, Toyoshima T, et al. In vivo evaluation of anodic TiO$_2$ nanotubes: an experimental study in the pig. J Biomed Mater Res B Appl Biomater 2009;89:165–71.

[54] Wang N, Li H, Lu W, Li J, Wang J, Zhang Z, et al. Effects of TiO$_2$ nanotubes with different diameters on gene expression and osseointegration of implants in minipigs. Biomaterials 2011;32:6900–11.

[55] Bjursten LM, Rasmusson L, Oh S, Smith GC, Brammer KS, Jin S. Titanium dioxide nanotubes enhance bone bonding in vivo. J Biomed Mater Res A 2010; 92:1218–24.

[56] von Wilmowsky C, Bauer S, Roedl S, Neukam FW, Schmuki P, Schlegel KA. The diameter of anodic TiO$_2$ nanotubes affects bone formation and correlates with the bone morphogenetic protein-2 expression in vivo. Clin Oral Implants Res Doi: 10.1111/j.1600–0501.2010.02139.x, in press.

[57] Yuan H, Fernandes H, Habibovic P, de Boer J, Barradas AM, de Ruiter A, et al. Osteoinductive ceramics as a synthetic alternative to autologous bone grafting. Proc Natl Acad Sci U S A 2010;107:13614–9.

[58] Anderson JM, Kushwaha M, Tambralli A, Bellis SL, Camata RP, Jun HW. Osteogenic differentiation of human mesenchymal stem cells directed by extracellular matrix-mimicking ligands in a biomimetic self-assembled peptide amphiphile nanomatrix. Biomacromolecules 2009;10:2935–44.